Development and Experimental Validation of a Control-Oriented Empirical Exhaust Gas Temperature Model

2020-24-0008

Development and Experimental Validation of a Control-Oriented Empirical Exhaust Gas Temperature Model

Author, co-author (Do NOT enter this information. It will be pulled from participant tab in MyTechZone)

Affiliation (Do NOT enter this information. It will be pulled from participant tab in MyTechZone)

Abstract

Modern turbo-charged downsized engines reach high values of specific power, causing a significant increase of the exhaust gas temperature. Such parameter plays a key role in the overall powertrain environmental impact because it strongly affects both the catalyst efficiency and the turbine durability. In fact, common techniques to properly manage the turbine inlet gas temperature are based on mixture enrichment, which causes both a steep increase in specific fuel consumption and a decrease of catalyst efficiency. At the test bench, exhaust gas temperature is typically measured using thermocouples that are not available for on-board application, and such information is processed to calibrate open-loop look-up-tables. A real-time, reliable, and accurate exhaust temperature model would then represent a strategic tool for improving the performance of the engine control system.

In this work, a novel analytical approach for the calculation of the exhaust gas temperature under steady-state conditions has been investigated and experimentally validated. An empirical control-oriented model has then been developed by incorporating the description of thermocouple dynamics, making it reliable for real-time application also under transient conditions.

At first, the control-oriented empirical model is introduced, describing how the polynomial approach used in a previous work of the authors has been applied to reproduce the steady-state thermocouple measurement. Then, a real-time compatible thermocouple dynamics model is proposed, and the calculated values are compared with the thermocouple signal under dynamic conditions.

In the last section of the paper the computational cost to execute the model is evaluated as the ratio between real and execution time. In this way the compatibility with on-board, real-time applications is finally demonstrated.

Introduction

Exhaust temperatures models are widely used in the automotive field and are typically implemented in Engine Control Units (ECUs). An accurate estimation of such parameters over the entire engine operating range for both steady-state and transient conditions is needed in order to prevent turbine failure in turbo-charged engines, and in general to optimize the after-treatment system efficiency, as highlighted by Fu and Chen [1]. The latter reason is particularly meaningful for modern three-way catalysts that work properly in a limited temperature range. Outside such temperature interval there is an evident drop for both conversion efficiency (for lower temperature values) and catalyst useful life (for higher temperature values). As well-known, the latest emission regulations for passenger cars are forcing engine manufacturers to achieve maximum efficiency for both the combustion process and the after-treatment systems [2]. Moreover, the exceedance of the maximum gas temperature at turbine inlet must be avoided, to prevent turbine failure. For such reasons, an accurate and reliable exhaust temperature model is a key tool in managing the main control levers to achieve desired engine-out gas temperature. The most widespread Spark-Ignition (SI) engine strategy for catalyst heating is spark retardation, while common techniques to lower exhaust gas temperatures are both the use of non-stoichiometric Air-to-Fuel Ratio (AFR) and load limitation, as well explained in [3]. For the mentioned control strategies, the engine-out temperature calculation is typically coupled with models for the estimation of the catalyst thermal behavior.

Majority of modelling effort found in literature deals with catalyst warmup and efficiency prediction and with temperature calculation at the turbine inlet [4, 5]. Some works develop methods based on 1-D approach that solve mass-energy balance equations for every sub volume within which exhaust pipes are divided. For example, the physics-based 1-D thermocouple model described in [6] outputs the estimated temperature by solving the thermal balance related to the heat exchanged by convection between exhaust gases and the thermocouple tip, and by conduction and radiation with the pipe wall. Nevertheless, such method is not compatible with RT application due to the high computational effort needed to solve the energy balance equation and this makes such 1-D models typically more suitable for engine components design and for the development and validation of custom control algorithms via Software-in-the-Loop simulation. On the other hand, accurate knowledge of temperature distribution during the engine cycle allows to highlight further criticisms for turbine but such kind of studies needs the calibration and validation of 3-D CFD models [7, 8, 9]. Instead, focus of this work is the real-time exhaust gas temperature modelling for SI engines. An innovative analytical approach is described in detail and an empirical model is developed and validated comparing the signals of the Thermocouples (TCs) installed in the engine exhaust manifold, with the modelled ones. Such model is based on the identification of appropriate polynomial functions to interpolate exhaust temperature values measured under steady-state operating conditions. Polynomial fittings of temperatures recorded in standard conditions (mapped values for both SA and lambda) do not consider the effects of deviations in SA or lambda targets under real engine operation. For

such reason, the sensitivities to combustion phase and AFR are modelled through polynomial functions that scale the modelled temperatures as a function of SA or lambda deviations with respect to the nominal values. A similar mathematical approach was presented in a previous work by the authors [10] in which the main combustion indexes (such as the 50% Mass Fraction Burnt Angle, or MFB50, the maximum in-cylinder pressure, and the Indicated Mean Effective Pressure or IMEP) are modelled using polynomial equations. The major advantage of the analytical approach is an extremely low computational effort required to run the resulting model, which makes it particularly suitable for Real-Time (RT) applications. Lookup Table calibration or artificial Neural Network (ANN) may be considered as valid alternatives to the polynomial method, and they represent the state-of-the art approaches [11]. However, it can be stated that limited literature in 0-D exhaust gas temperature modelling exists, while 1-D and 3-D modelling have been more extensively explored [12, 13]. The analytical model, based on polynomial functions, is one of the innovative contributions of this work since it ensures a higher accuracy (due to the absence of discretization of the independent variables) and a lower calibration effort. In fact, when the polynomial degree of the fitting function is fixed, the number of calibration points can be significantly reduced. More generally, if the Lookup-Table and ANN-based models can be associated to the typical *black-box* approach, it can be asserted that the proposed methodology is more similar to a *grey-box* one, due to preliminary analysis of variable trend.

A simplified methodology to reproduce the TC temperature signal also for transient conditions is the focus of the second part of paper. The TC output and dynamics are affected by three main factors: TC lumped thermal capacity, conduction heat transfer between TC tip and pipe wall through the mounting support, and radiation heat transfer between TC and the surrounding pipe wall [14]. While TC thermal inertia has no effects in steady-state conditions, and it acts like a first-order system when the engine point changes, conduction and radiation heat transfers affect both steady-state and transient TC output. Indeed, they typically introduce a negative offset on the stationary measured temperature, causing a systematic underestimation [15]. Nevertheless, the steady-state TC measurement can be considered significant for the purpose of this work because the limit values provided by turbine and catalyst manufacturers are defined by using thermocouples in steady-state conditions. This means temperature limits for such components already include the negative offset given by performing measurements with TCs, thus, they can be taken as reference. Under dynamic conditions, the TC thermal capacity is probably the most influent factor on the initial response, and it may be synthesized by its time constant. Moreover, the conduction heat transfer between the TC and the walls of the exhaust runner additionally deviates the TC tip temperature from that of the exhaust gases under dynamic conditions, slowing down the reaching of the steady state value [16]. A similar effect is due to the heat transfer caused by radiation between the TC tip and the pipe wall, which is particularly relevant since the heat transfer is proportional to the temperature difference raised to the 4th power. Therefore, conduction and radiation heat transfers between TC and pipe wall, together with TC thermal inertia and the mixing of the novel exhaust gases ejected from the combustion chamber with those within the runners, cause the resulting experimental trend of temperature readings under transient conditions. Such exhaust gas mixing and the effect of the TC time constant are responsible for the initial fast part of the TC response during a steep temperature transition. The slower behavior is, instead, given by conduction and radiation with the pipe wall [17, 18]. The model proposed by the authors includes two Moving Averages (MAs) that were calibrated to reproduce the resulting trend of the TC signal. The analytic exhaust gas temperature model coupled with the TC dynamics model are validated through the comparison between the calculated values and the measured ones, for both steady-state and transient conditions, and the error is evaluated.

Experimental Campaign

Experimental tests were carried out on an 8-cylinder, 3.9 liter GDI Turbo-Charged engine. The main features of this engine are listed in Table 1. Data used for development and calibration of the model were recorded performing spark and lambda sweeps on the entire engine operating range, and the mean cylinder was considered for the indicating indexes. The tested operating conditions are shown in Figure 1. For each engine point, the spark sweep was performed while maintaining the mapped lambda value, and the measurements were performed in steady state conditions, including about 200 engine cycles for every operating point. An analogous approach was used for lambda sweeps: the AFR value was changed while fixing a given value of the MFB50 and engine load, via adjustment of the actuated SA and the requested torque, respectively. Moreover, some transient operating conditions were tested while the bench signals (such as the exhaust temperature readings from the TCs, engine speed and load) as well as the main combustion and control indexes were logged for the validation process. Such data were collected on engine points that are not included in the initial calibration database, to also check the reliability of the proposed methods. The exhaust runners and manifold were instrumented with Mineral-Insulated-Metal-Sheathed (MIMS) thermocouples. The main combustion indexes were calculated from the in-cylinder pressure signals: CHAMPION charge amplifier and OBI-M2 indicating system by Alma Automotive were used for signal conditioning and acquisition. Indeed, each cylinder was equipped with a piezoelectric transducer, and the signal was sampled with a frequency of 200 kHz. The calculation of MFB50, IMEP and Pmax uses the low-pass filtered pressure trace. Cut-off frequencies of the filter were identified for this specific application, but they cannot be disclosed for confidentiality reasons. For the same motivation, all the variables and parameters were normalized or partially offset in the paper.

Table 1. Engine characteristics.

Displaced volume	3.9 L (8 cylinder)
Stroke	82 mm
Bore	86.5 mm
Connecting Rod	143 mm
Compression ratio	9.45:1
Number of Valves per Cylinder	4

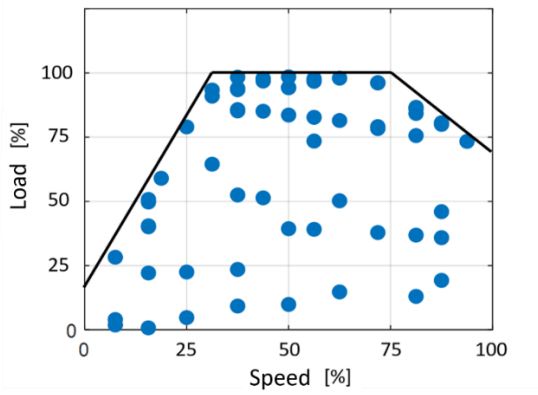

Figure 1. A total of 60 engine points on the Speed-Load range were tested for the calibration process. For each point a spark sweep was performed, and for 14 of these, a lambda sweep was carried out.

Analytical Model

The proposed model has been calibrated to minimize errors between the experimental exhaust manifold gas temperature and the calculated one under steady-state conditions. The temperature of gases within the exhaust manifold is considered.

In the following section the development of the analytical model and the thermocouple dynamics model are thoroughly described. It is important to mention that the empirical model of the TC dynamics was developed in order to improve the quality of the calculated values when compared against experimental signals. This becomes unnecessary when the aim of the model is to determine the exhaust gas temperature on-board the vehicle, for instance within a RT control strategy for a Turbo-Charged engine that must prevent the turbine failure through mixture enrichment. In this case the implementation of the TC dynamics model acts as a first-order system, hence it causes the calculation of temperatures that are coherent with TC output but lower than the "real" ones during fast transient conditions characterized by increasing power (from low to high load), according to what stated in the introduction. This means that for the prevention of turbine overheating such model should always calculate the real gas temperature, rather than the measured temperature. On the contrary, the TC dynamic model is needed for the exhaust temperature model validation under transient conditions because the TC signal is the only measurable feedback of such engine variable. A comparison between the modelled and the logged temperatures without the contribution of the TC dynamics representation would only be meaningful for steady-state conditions.

The proposed approach provides the analysis of the effects that the engine operating condition (both engine speed and load), the combustion phase (defined through the MFB50 index that represents the angular value for which the normalized Cumulative Heat Release curve meets the 0.5 value) and the lambda value produce on the exhaust gas temperature. Moreover, such effects were studied separately and included in the model by adding each contribution to reach the temperature for fixed engine speed, load, MFB50 and lambda. In other words, such model was developed by using the effects-separation method: the steady-state gas temperature, estimated for a given engine operating point, with the calibrated lambda value and a reference value of MFB50, is multiplied by two functions that are designed to adjust the reference temperature when the AFR or the combustion phase deviate from nominal conditions.

Figure 2 shows the block-layout of the analytical model, as implemented in Simulink. The reference temperature (obtained for the reference values of combustion phase and lambda) is calculated with the T_EXH_REF block, that uses the engine speed (ES) and the engine load (EL) as inputs. EL is defined as the relative air charge inside the combustion chamber, independent of engine displacement, and it is calculated as the ratio between the actual air mass in the combustion chamber and the air mass at normalized conditions (Pref=1013hPa, Tref=273K). Such temperature is multiplied by two gains that consider the effect of a different MFB50 (MFB_GAIN block) and lambda (λ_GAIN block), respectively. The result of such product is the gas temperature within the exhaust manifold (i.e., the one that would be measured with a MIMS TC under steady-state conditions). The MFB50 index is calculated by an empirical model that was discussed in a previous work by the authors [10], in order to produce an algorithm that does not need indicating indexes as input, and can therefore be implemented in an engine controller. This makes the proposed approach a valid solution also for on-board applications. In the following paragraphs, each block of the analytical exhaust gas temperature model is described in detail.

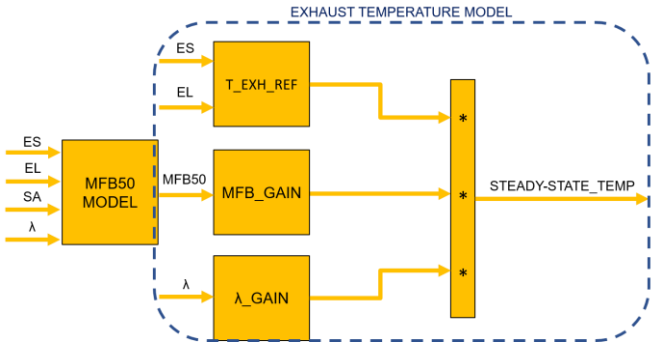

Figure 2. Block-layout of the exhaust gas temperature model. The reference temperature is multiplied by two factors that depend on MFB50 and lambda values respectively. The MFB50 model from [4] allows to calculate the combustion phase without the need for indicating signals.

Reference Temperature Model

Every spark sweep was carried out by applying wide SA variations while maintaining lambda at its calibrated value. In this way, it was possible to calculate exhaust gas reference temperatures on the entire engine operating range. These temperatures represent the ones that would theoretically be measured within the exhaust manifold under steady-state conditions, when lambda is equal to the mapped value and the normalized MFB50 is equal to a fixed reference value. MFB50 is evaluated in terms of arbitrary units (for which the unitary variation corresponds to a certain amount of crank angle degrees) while the temperatures were normalized with respect to the maximum and indicated as percentage values (considering degrees Celsius before normalization).The reference combustion phase was assumed equal to 2 because all the spark-sweeps were centered around such value . In this way, the calculation of the corresponding temperature was always done through interpolation of the experimental values, without performing an extrapolation that could be a source of error. The trend of these temperatures with respect to engine speed and load is shown in Figure 3, where the blue dots indicate the values calculated through the interpolation of adjacent experimental data and the surface represents the overall fitting function. The interpolation process is needed due to missing experimental temperature values for MFB50 exactly equal to 2. The effect caused by the combustion phase is then accurately excluded in this way from the reference temperature definition. With this function, the influence of the engine speed and load is introduced in the exhaust gas temperature model.

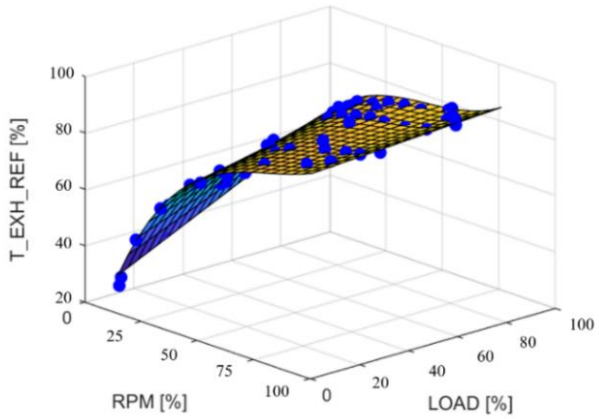

Figure 3. Trend of the reference temperatures (lambda=map, MFB50=2) on the normalized RPM-Load range. The blue dots represent values corresponding to the MFB50=2 calculated through the interpolation of the experimental data, while the surface is the *poly31* fitting function.

The choice of the polynomial order is carried out by identifying the optimal compromise between the fitting performance and the function complexity. If, by increasing the polynomial order, the accuracy improvement is negligible, the last formulation that guaranteed a significant performance step is chosen. More generally, the definition of the polynomial order is also driven by the analysis of the independent variable trend. The goodness of the fitting process has been evaluated through the R2 and the RMSE indexes defined by Equations (2) and (3) [19]. Table 2 collects polynomial order, R^2, and Root-Mean-Squared-Error (RMSE) for the reference temperatures (correlation and errors are evaluated between experimental and fitted values). The last polynomial order that guarantees an increment higher than 10^{-2} in terms of R2 is chosen for the fitting process. The importance of selecting the as low as possible polynomial order is not only related to the computational effort needed by the model execution. Indeed, major complexity comes from the numerical optimization of power function for final implementation in RT machine. Second or third power force programmer to declare the output of that function with a wide number of digits and this opposes the necessity to minimize the impact on RAM of Rapid Control Prototyping (RCP) system. Such effort must be as low as possible. The RMSE index is calculated for percentage quantities (normalized for confidentiality reasons). Thus, the output of Equation (3) is a percentage value. The nomenclature '*polylv*' indicates that the polynomial is characterized by a degree *l* for the first independent variable (X=engine speed) and a degree *v* for the second one (Y=engine load). All the possible order combinations were tested from *poly11* to *poly33*. Equation (1) represents the analytical form of the fitting function (*poly31*):

$$T\_EXH\_REF = p_{00} + p_{10}X + p_{01}Y + p_{20}X^2 + p_{11}XY + p_{30}X^3 + p_{21}X^2Y \quad (1)$$

In which:

- T_EXH_REF is the dependent variable
- X and Y represent engine speed and load
- p_{lv} is the coefficient for the element in which there is a degree l for X and a degree v for Y.

Equations 2 and 3 specify R^2 and RMSE analytical formulations, respectively:

$$R^2 = \left(\frac{\sum(c_i - \bar{c})(e_i - \bar{e})}{N\,(\sigma_c\,\sigma_e)}\right)^2 \quad (2)$$

$$RMSE = \sqrt{\frac{\sum(c_i - e_i)^2}{N}} \quad (3)$$

Where:

- N is the number of samples
- c_i/e_i is the generic calculated/experimental value
- $\bar{c}/\bar{e}$ is the calculated/experimental mean value
- σ_c/σ_e is the calculated/experimental standard deviation

Table 2. Sensitivity analysis to the fitting polynomial order, for the reference temperature. The green row highlights the best polynomial order.

Polynomial	R2	RMSE [%]
poly11	0.828	8.331
poly12	0.926	5.562
poly21	0.972	3.381
poly13	0.927	5.612
poly31	0.995	1.903
poly22	0.974	3.301
poly23	0.985	2.588
poly32	0.996	1.813
poly33	0.997	1.767

The robustness of this fitting process through a *poly31* polynomial was tested by reducing the number of engine points used for the calibration process and by verifying the performance on the total amount of experimental data. Figure 4 shows R^2 values for the fittings with a different number of used engine points: it is possible to highlight that the accuracy of the model does not significantly change when a lower number of Spark Sweeps is used for the calibration. By reducing the calibration data, the engine points are still selected in order to be spread out enough to cover the whole engine operating range.

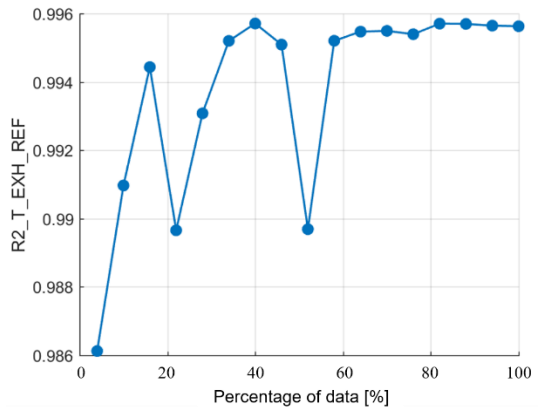

Figure 4. R^2 index calculated with a different number of experimental points used for the model calibration. The percentage values indicate the amount of engine points used for fitting procedure with respect to the entire database. 100% corresponds to 60 engine points (i.e. 60 spark sweeps), 20% to 12.

MFB50 Dependency Model

The next step in the development of the analytical model consists of the analysis of the spark-sweeps database and for each tested operating condition (fixed engine speed and load) the exhaust gas temperature trend for the mean cylinder was studied and fitted with a polynomial equation with respect to the combustion phase. Figure 5 displays the average temperature for different SA values recorded under steady-state conditions (blue dots) and the fitting curve (red line), for the engine point at 4000 rpm and full load.

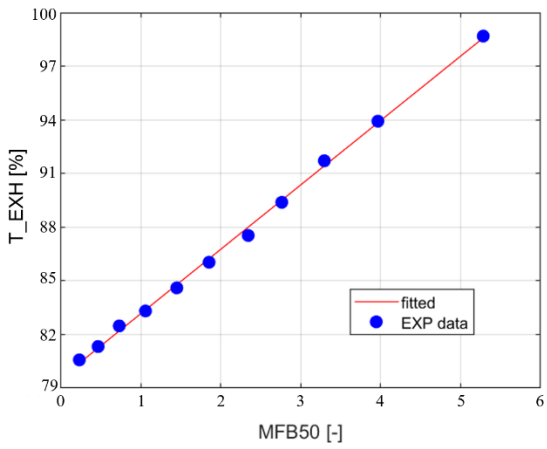

Figure 5. Exhaust manifold gas temperature as a function of combustion phase (MFB50), for fixed engine speed and load. The blue dots and the red line represent the experimental values logged for different values of the SA and the fitting polynomial function respectively.

As observable from Figure 5, the polynomial degree is equal to 1 (linear function), due to the accuracy already provided by such kind of function. For such fitting process, the mean R2 values and the RMSE indexes for all engine points have been collected in Table 3.

Table 3. R2 and RMSE mean values for all spark-sweeps. The exhaust gas temperature was fitted as a function of MFB50 with a linear polynomial function, for each tested engine speed and load.

R2	RMSE [%]
0.987	0.472

The function chosen for the fitting has the simple form shown in Equation (4):

$$Texh = p_0 + p_1 MFB50 \quad (4)$$

Where:

- $Texh$ is the dependent variable (the gas temperature in the exhaust manifold, as measured with the TC)
- $MFB50$ is the combustion phase
- p_l is the coefficient that multiplies the combustion phase at the l power.

This polynomial function can be considered as a corrective function of the modeled temperature when the combustion phase changes. In fact, by fixing an arbitrary reference value of MFB50 and normalizing the polynomial function with respect to temperature value that corresponds to such reference, it is possible to obtain a new function that defines the multiplying factor. In other words, when MFB50 is equal to the reference value the gain is equal to 1, while if MFB50 is lower or higher than the reference, the gain is lower or higher than 1, respectively. Figure 6 shows the same data as in Figure 5 after the normalization with respect to the value of the temperature that corresponds to the MFB50 equal to 2. The red line represents the fitting function defined by Equation (5):

$$MFB\_GAIN = p_{0\_MFB} + p_{1\_MFB} MFB50 \quad (5)$$

Where p_{0_MFB} and p_{1_MFB} are the coefficients of the MFB_GAIN function. This procedure allows to identify the gas temperature along the exhaust manifold for fixed operating conditions (engine speed, load, the calibrated – or nominal – lambda value, and any given value of the combustion phase), according to the following Equation (6):

$$Texh = T\_EXH\_REF(ES, EL) * MFB\_GAIN(MFB50) \quad (6)$$

Where T_EXH_REF indicates the reference temperature, as defined by Equation (1) in the previous section of the paper, at reference (mapped) SA and AFR, for any given engine speed and load (*ES* and *EL* respectively). The new term in Equation (6) implements the combustion phase dependency, which is now added to the model.

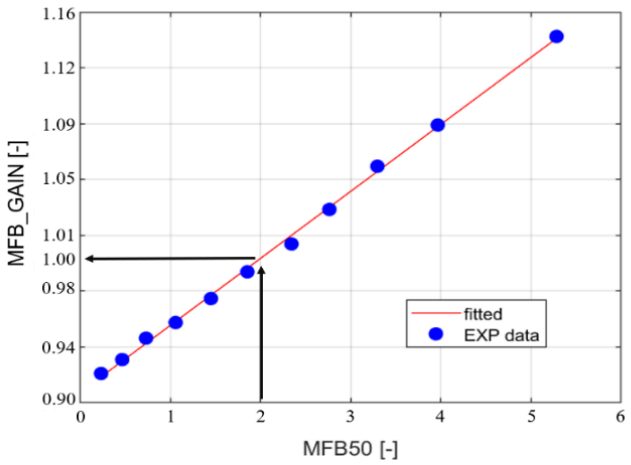

Figure 6. Exhaust gas temperature is normalized with respect to the value in correspondence with the reference MFB50. Thus, the red line represents the correction function of the temperature for a given operating condition.

The MFB_GAIN fitting function was then considered and the coefficients p_{0_MFB} and p_{1_MFB} were hence separately identified for all the 60 tested engine points. Such analysis demonstrated that the numerical values for gains and offsets are all very similar. This means that the trend of such coefficients with respect to the engine speed and load can be neglected. This observation allows the use of mean p_{0_MFB} and p_{1_MFB} on the entire engine operating range. Figures 7 and 8 display such values for each test and the indicated numbers refer to the normalized temperatures fitted with respect to the MFB50 values considered as arbitrary unit. In such figures there are two red dashed lines that indicate the upper and lower limit of the rounded dispersion of data.

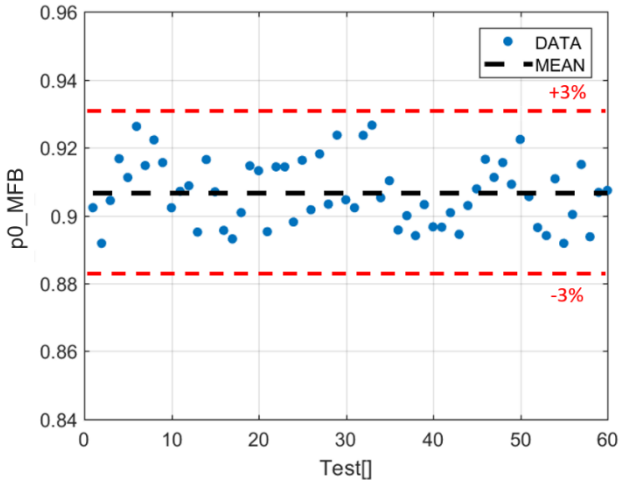

Figure 7. Numerical values of coefficient p_{0_MFB} identified for each spark-sweep. The black dashed line indicates the mean value, while the two red dashed lines represent the upper and lower limit of the rounded dispersion of data, which lie within +-3%.

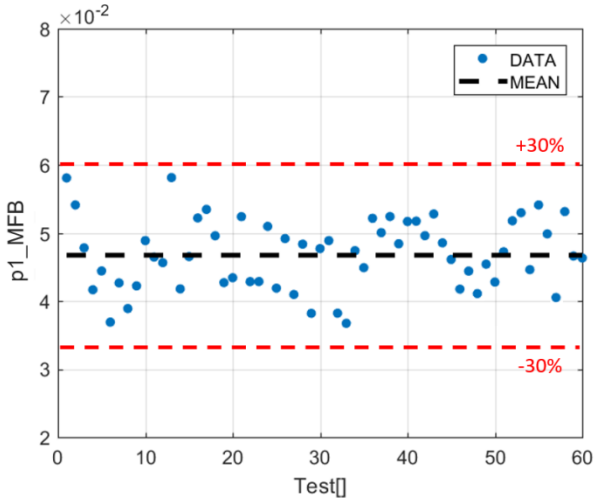

Figure 8. Numerical values of the coefficient p_{1_MFB} for each spark-sweep. The black dashed line indicates the mean value, while the two red dashed lines represent the upper and lower limit of the rounded dispersion of data, which lie within +-30%.

The absolute percentage error between each fitting function (the specific values of MFB50_GAIN function calculated for each spark sweep) and the one that derives from the approximation of the coefficients with their mean value (the mean MFB50_GAIN function) were then evaluated. The error using the mean value is equal to 0.43% and this result legitimates such simplification.

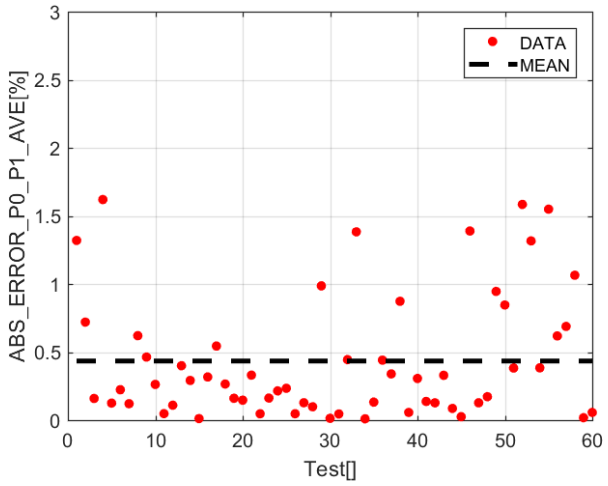

Figure 9. Absolute error for all the spark sweeps, given by the approximation of coefficients p_0 and p_1 with their corresponding mean value. The mean value of the error is equal to 0.43% and this result confirms the possibility of simplifying each fitting function with the average polynomial coefficients.

A sensitivity analysis was therefore carried out by imposing a fixed error on p_{0_MFB} and p_{1_MFB} and studying the resulting error on the MFB_GAIN. Table 4 collects the mean error on the MFB_GAIN function when a given percentage error is imposed on each coefficient. This study demonstrates that an approximated gain of the linear polynomial (the coefficient p_{1_MFB}) causes a much lower error on the resulting function than the one obtained with the same percentage error on the offset (the coefficient p_{0_MFB}). This observation allows to clarify how the approximation of both

coefficients has the same effect on the final error, even if the dispersion of p_{1_MFB} is ten times higher.

Table 4. Sensitivity analysis of the MFB_GAIN function to the error imposed on the p_{0_MFB} and p_{1_MFB} mean values.

Error on P0_MFB [%]	Mean Error on MFB_GAIN [%]
10	1.44
20	5.97
30	9.50
40	14.03
50	18.57
60	23.10
Error on P1_MFB [%]	**Mean Error on MFB_GAIN [%]**
10	0.04
20	0.09
30	0.15
40	0.19
50	0.25
60	0.31

Lambda Dependency Model

The methodology used for AFR impact on exhaust gas temperature variations is similar to the approach used for the combustion phase. The experimental database consists in 14 lambda sweeps carried out on a portion of the engine points represented in Figure 1. Tests were performed mainly on the portion of the engine operating filed characterized by the highest speed and load, because it is in this portion of the engine map that turbine inlet temperatures need to be closely controlled. Thus, in these operating conditions it is particularly important to guarantee an accurate estimation of exhaust gas temperature. Figure 10 shows the engine points on which lambda sweeps were carried out. Such tests were performed while controlling both combustion phase and engine load. In fact, combustion phase and load are affected by AFR but, during this kind of test, it is important to separate the effect of AFR on the exhaust gas temperature from those of MFB50, engine speed and load. This was achieved by checking the effective load and the combustion phase when lambda was changed, by adjusting SA to maintain MFB50 close to the normalized reference value (equal to 2), and by keeping constant IMEP. Indeed, as already mentioned in the first section of this paper, the proposed approach implements the effects-separation method. Such experimental campaign needs to collect data to analyze mixture quality effects on exhaust temperature, excluding the influence of combustion efficiency that depends on combustion phase. For this reason, MFB50 is maintained equal to the reference value used to calibrate the reference temperature model.

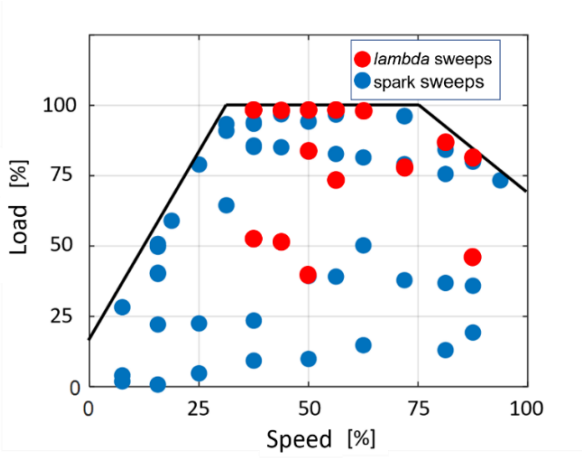

Figure 10. Red dots indicate the 14 engine points in which lambda sweeps were performed. The blue points represent the operating conditions for which a spark-sweep was carried out.

Exhaust gas temperatures recorded during steady state lambda sweeps were described through a linear polynomial. Temperatures were normalized with respect to mapped lambda conditions. Reference temperature for the calibrated lambda has to coincide with the value recorded during the spark sweep on the same engine point because lambda sweeps were carried out maintaining the MFB50 equal to 2. Figure 11 shows the function of the corrective factor that has unitary value when lambda matches the mapped value. The trend of the normalized exhaust gas temperatures on lambda was described through a linear function, even if for some engine points a degree 2 equation could improve R2 and RMSE indexes. Nevertheless, the magnitude of the improvement is weighted with the computational cost increase due to the calculation of some squared quantities that strongly impacts on the numerical optimization cost of the algorithm when it has to be implemented in a RT machine or in a ECU. For this reason, a simplified approach is preferred.

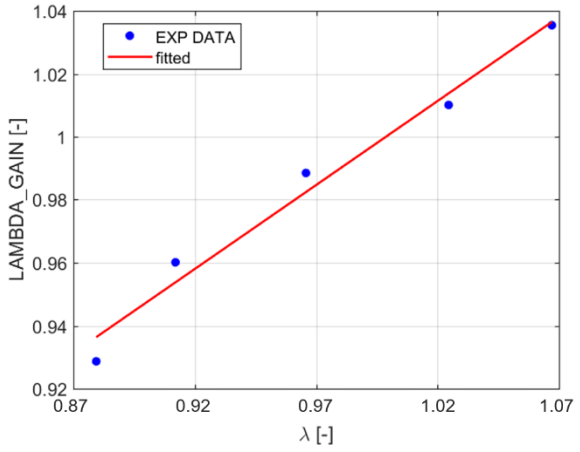

Figure 11. Exhaust gas temperatures were normalized with respect to the reference value. Blue dots indicate the normalized gas temperature values while the red line represents the corresponding fitting function.

The LAMBDA_GAIN function is defined by Equation (7):

$$LAMBDA\_GAIN = p_{0\_LAMBDA} + p_{1\_LAMBDA}\lambda \quad (7)$$

Where p_{0_LAMBDA} and p_{1_LAMBDA} are the coefficients of the LAMBDA_GAIN function. Thus, introducing lambda dependency, the exhaust gas temperature is calculated according to the following Equation (8):

$$Texh = T\_EXH\_REF(ES, EL) * LAMBDA\_GAIN(\lambda) * MFB\_GAIN(MFB50) \quad (8)$$

Where T_EXH_REF indicates the reference temperature, that is defined as a function of engine speed (ES) and load (EL)in nominal conditions. The selected LAMBDA_GAIN function is characterized by a polynomial degree equal to 1 and the accuracy of the fitting process was evaluated through R2 and RMSE indexes. The mean values for all the 14 tested engine points are collected in Table 5.

Table 5. R2 and RMSE indexes mean values. The normalized exhaust gas temperatures were described with a linear polynomial function.

R2	RMSE [%]
0.971	0.702

Coefficients p_{0_LAMBDA} and p_{1_LAMBDA} were analyzed and the corresponding mean values were calculated. The error caused by the approximation of all the polynomials with the average one was assessed: figures 12 and 13 display the values of the coefficients p_{0_LAMBDA} and p_{1_LAMBDA} for each lambda sweep and the value of the rounded maximum percentage dispersion.

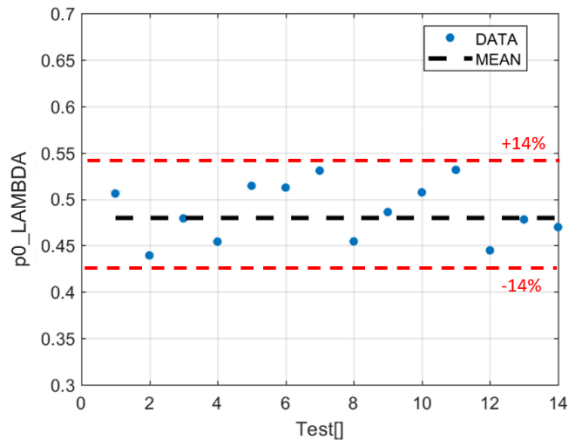

Figure 12. Numerical values of the coefficient p_{0_LAMBDA} for each *lambda* sweep. The black dashed line indicates the mean value, while the two red dashed lines represent the rounded limits of the data dispersion, which lie within +-14%.

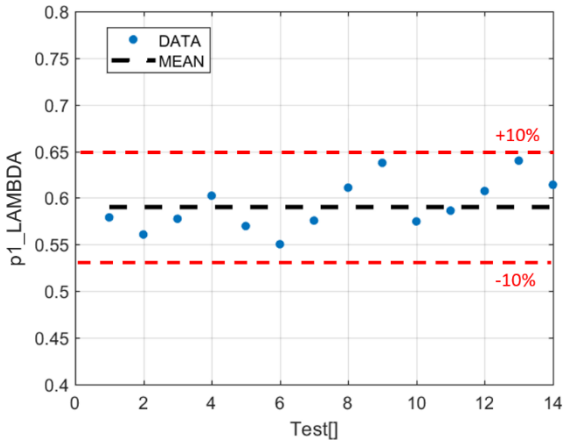

Figure 13. Numerical values of the coefficient p_{1_LAMBDA} for each *lambda* sweep. The black dashed line indicates the mean value, while the two red dashed lines represent the rounded limits of the data dispersion, which lie within +-10%.

As for the MFB50_GAIN block, the accuracy of the mean function (the function defined by the mean offset and gain) was checked by calculating the error for each lambda sweep and carrying out a sensitivity analysis of the LAMBDA_GAIN to the imposed error on the coefficients p_{0_LAMBDA} and p_{1_LAMBDA}. The error is defined as the mean absolute value of the difference between each LAMBDA_GAIN function obtained for every lambda sweep and the mean function. Figure 14 shows such error for each test and Table 6 collects data about the sensitivity analysis.

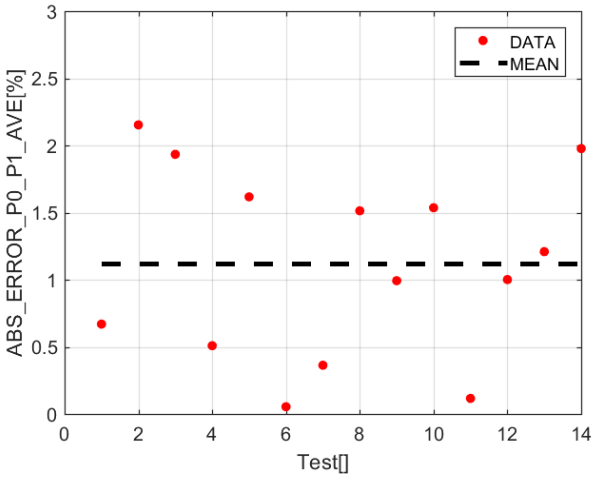

Figure 14. Absolute error for each lambda sweep given by approximation of coefficients p_{0_LAMBDA} and p_{1_LAMBDA} with the corresponding mean value. The mean error is equal to 1.11%: this result confirms the possibility to simplify each fitting function with the average polynomial.

Table 6. Sensitivity analysis of LAMBDA_GAIN function to the error imposed on p_{0_LAMBDA} and p_{1_LAMBDA} mean values.

Error on P0_LAMBDA [%]	Mean Error on MFB_GAIN [%]
10	0.77
20	1.51
30	2.25

40	3.00
50	3.72
60	4.46
Error on P1_LAMBDA [%]	**Mean Error on MFB_GAIN [%]**
10	0.23
20	0.98
30	1.63
40	2.41
50	3.20
60	3.99

Model Validation under Steady-State Conditions

The complete algorithm composed by the reference temperature model, the MFB_GAIN, and the LAMBDA_GAIN functions, was then validated through comparison of steady-state temperatures related to the whole experimental database and the corresponding modelled values. The error between all recorded exhaust gas temperatures (for both spark and *lambda* sweeps) and the values calculated by supplying the model with the mean control and indicating parameters (engine speed, load, MFB50 and lambda) is shown in Figure 15. Every point represents the difference between the steady state TC measurement and the calculated value, for each engine operating condition. Results confirm the accuracy of the model for all tested engine speed-load conditions, and also for all the actuated SA and *lambda* values.

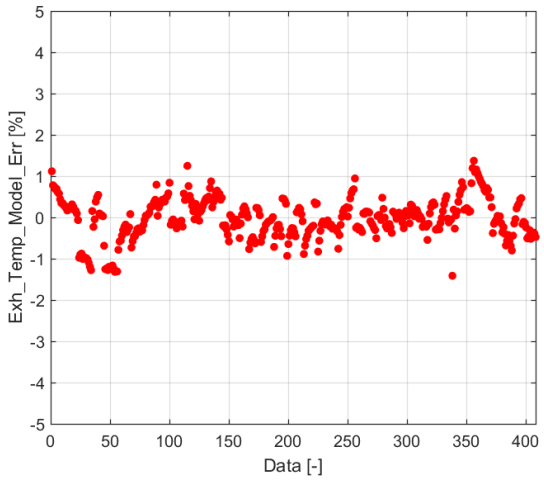

Figure 15. Error between measured and modelled steady-state exhaust gas temperatures

TC Dynamics Model

This paragraph is dedicated to the development of the TC dynamics model and the method used for its implementation within Simulink. Such model uses the steady-state exhaust gas temperature as input, and it applies a calibratable filter to reproduce TC dynamics during transient conditions. In this way the calculated temperature can be directly compared with the TC signal. Figure 16 shows a qualitative trend of the gas temperature measured with a TC when the engine operating condition is changed drastically. The real exhaust gas temperature changes quickly but the TC output is affected by its own dynamics which include mainly its time constant, conduction and radiation between TC tip and manifold wall. Moreover, as introduced in the first part of this work, also gas mixing within exhaust runners and manifold influences the temperature trend under transient conditions.

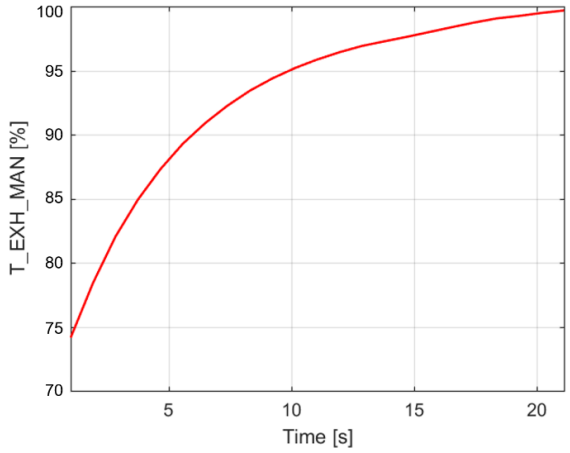

Figure 16. Normalized TC temperature trend during a fast transient condition.

The behavior of the TC output is initially characterized by a fast response, followed by a slower transient to reach steady state [17]. The TC time constant and the gas mixing within the exhaust manifold cause the faster part of the dynamics, while conduction and radiation phenomena are responsible for the slower one. The approach used to reproduce such trend is based on the algebraic sum of the output of two different filters, that were implemented in the form of two weighted moving averages. The one with the lower weight corresponds to the faster filter, and the one with the higher weight corresponds to the slower one. Through a proper calibration it is possible to reproduce TC dynamics. For both moving averages the weight applied to the current value was defined as the value complementary to 1 w.r.t. the calibrated weight. The output of each moving average is then weighted further before summing the faster and the slower contribution, in order to calculate the final modeled temperature. These last two weights are again defined in such a way that their sum is equal to 1.

The calibration parameters of such TC dynamic model are the weight of the old value for the faster and the slower moving average, and the one relative to the sum of these two contributions. Figure 17 and 18 display the Simulink representation of the TC dynamics model. Figure 17 shows how the moving averages were implemented in the simulation environment, and the calibratable weight is highlighted. Such parameter is defined as a percentage number and it indicates the influence of the old value in the calculation of the output, with respect to the current value. The difference between such weight divided by 100 and the constant 1 defines the weight applied to the current value. A switch block was introduced to avoid the propagation of an inconsistent output. Figure 18 shows an overview of the sum of the output of the faster and slower moving averages. The calibratable weight was arbitrarily assigned to the output of the slower filter.

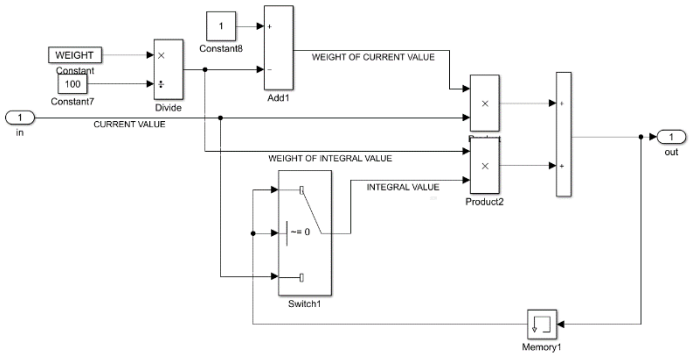

Figure 17. Simulink block scheme used to implement moving averages.

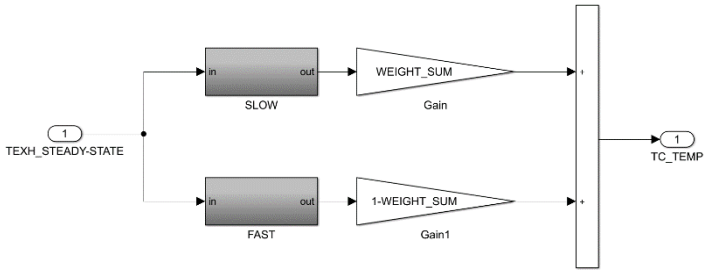

Figure 18. Simulink blocks used for the sum of moving the average outputs.

Model Validation under Transient Conditions

The TC dynamics model was coupled with the analytical one and the complete model was validated by comparing the measured and the calculated exhaust manifold temperatures under transient conditions. The parameters of the TC dynamic model were calibrated with dedicated tests. However, it is important to mention that the focus of this paragraph is mainly to validate the analytical exhaust gas temperature model, and the TC model is useful in order to have an output signal directly comparable with the actual TC reading. The reason is that the final purpose of this model is to be implemented in a control strategy for the RT estimation of the gas temperature at the turbine inlet, and for this kind of application the TC dynamics model can be excluded, due to the underestimation of the gas temperature under transient conditions. The experimental database used for the validation of the complete models is composed of two tests performed at the test bench, characterized by different engine speed and load transients. Moreover, some SA and lambda steps were externally imposed to verify the quality of the combustion phase and AFR dependencies modelling.

The steady-state exhaust manifold temperature calculated by the analytical model was used as input for the TC dynamic one. Figure 19 shows the block scheme of the complete model.

Figure 19. The exhaust manifold temperature model was coupled with the TC dynamic model in order to reproduce the TC signal also under transient conditions.

The engine and the complete analytical model were supplied with the same speed, load, SA, and lambda profiles, and the experimental and modelled gas temperatures were compared. Two different tests were carried out in order to cover the high speed-high load operating range. This is because such area is the critical one for inlet turbine temperature: an accurate prediction of the exhaust gas temperature is crucial. Tests under transient conditions allow to stress the model also on engine points that are not included in the calibration database. Achieving a limited estimation error on the entire test is a further demonstration of the validity of the proposed method.

Results and Discussion

Figures 20 and 22 show the main actuations of each test (engine speed, load, SA, and lambda), while in Figures 21 and 23 the corresponding calculated and experimental temperatures are shown. As for MFB50, also SA is evaluated in terms of arbitrary units, for which the unitary variation corresponds to a certain amount of crank angle degrees. Error in figures 21 and 23 is calculated as the difference between experimental and calculated value.

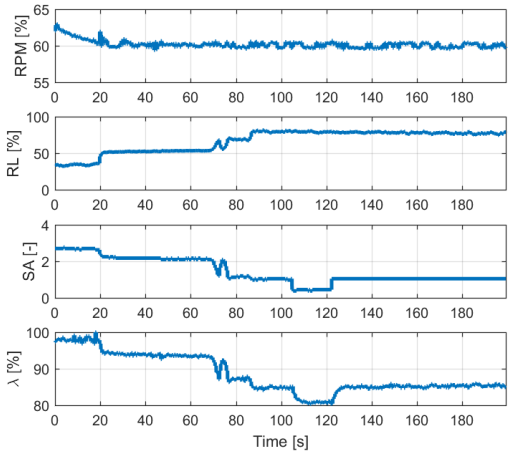

Figure 20. Normalized Engine speed, load, SA, and lambda profiles for test 1.

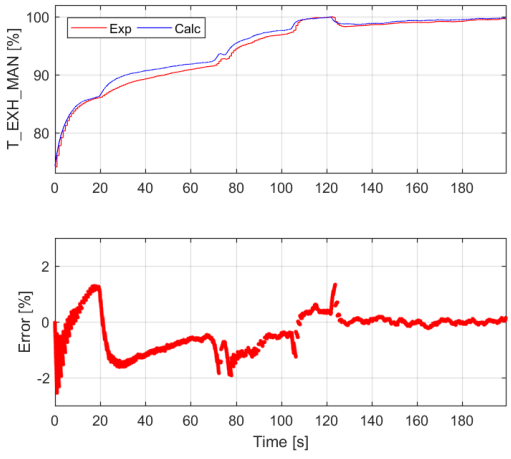

Figure 21. Performance of the complete analytical model under transient conditions (test 1).

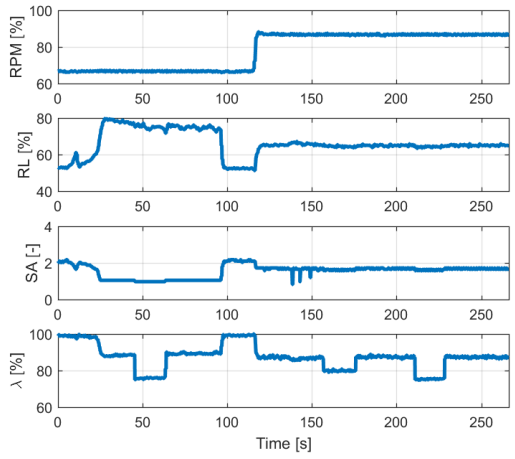

Figure 22. Normalized Engine speed, load, SA, and lambda profiles for test 2.

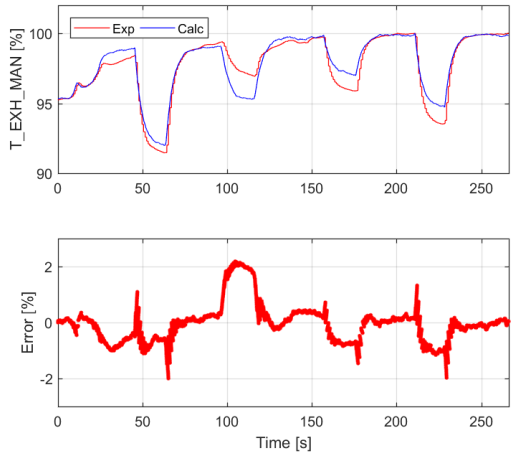

Figure 23. Performance of the complete analytical model under transient conditions (test 2).

The results clearly confirm the high accuracy and reliability of the complete model. The error is typically within the range +-2%. However, it can be observed that the widest percentage error is caused by lambda steps, especially for the test 2. This is due to the linear trend of the LAMBDA_GAIN function but, as anticipated above, the extremely low value of the error does not justify an increase in the function complexity. In fact, the mean absolute error for the validation tests is equal to 1.35%, proving the high accuracy of the proposed approach. Due to the type of tests designed for the model validation, this value represents the average error obtainable over the entire operating range. The discontinuous shape exhibited by the TC signal during fast transients is due to the low frequency temperature sampling, and this causes an unavoidable gap between the calculated and the experimental signals. This means the error can be reduced further by increasing the acquisition rate.

The ratio between the actual and the model execution time interval is equal to 312. This implies that such model can be executed 312 times faster than real time, on a standard laptop equipped with an Intel Core i7 6600U CPU and 8GB of RAM. Such result demonstrates that the developed model is particularly suitable to be implemented in a RT control strategy, due to the extremely low computational effort required for its execution.

Conclusions and Future Works

A novel approach for the exhaust gas temperature modelling was investigated in this work. An empirical method described in a previous work by the authors was extended in order to obtain an accurate and reliable model for the exhaust gas temperature estimation under steady-state conditions, and an analytical model of the sensor dynamics was developed so as to extend the validity of the approach also to transient conditions. The dependencies to SA and lambda were introduced and a wide experimental database was collected for the calibration process. Moreover, the robustness of the proposed approach was demonstrated through a sensitivity analysis of the model accuracy w.r.t. the number of engine points used for the calibration.

The analytical approach is based on the analysis of the effects of the main control parameters (SA and lambda) that influence the exhaust gas temperature, and on their modelling by implementing the effects-separation method. The effects of engine speed and load on the exhaust manifold temperature were captured with a relatively low-degree polynomial function that reproduces the experimental data for fixed MFB50 and for the mapped values of lambda. Linear polynomial functions for the calculation of the multiplying factors to adjust the reference temperatures with respect to a different MFB50 or lambda were then calibrated and added to the Simulink model. The proposed empirical approach guarantees a high level of accuracy, with percentage errors included within the range of +-1% under steady-state conditions. Such result is even more remarkable considering the extremely low level of complexity of the resulting code. The very simple modelling approach makes such model particularly suitable to be implemented in control applications designed to manage the turbine inlet gas temperature in Turbo-Charged engines.

A control-oriented TC dynamics model was also introduced to reproduce the TC signal also under transient conditions. In fact, TC dynamics is affected by physical phenomena such as the TC thermal inertia, gas mixing within exhaust runners and manifold, and conduction and radiation heat exchanges between the TC tip and the pipe wall, factors which act like low-pass filters during fast temperature transients. The TC behavior was modelled with two weighted moving averages that were calibrated to work like a faster and a slower response on the input signal, respectively. The outputs of these filters were then weighted and added in order to obtain the resulting signal. Nevertheless, the TC dynamics model was developed and implemented for simulation purposes only, because it leads to underestimating the real exhaust gas temperature under transient conditions. For this reason, such model would be excluded from a possible implementation in a RT control strategy.
The TC dynamic model was finally coupled with the exhaust gas temperature model and calibrated to minimize the error between the experimental and the calculated signal. The complete model was tested under transient conditions, comparing the TC and the modelled temperature profiles, and calculating the percentage error. Two different tests were carried out at the test bench, by varying the main parameters that influence the exhaust gas temperature, i.e. engine speed and load, SA, and lambda. Also in this case, the accuracy and the robustness of the complete model was demonstrated, registering absolute percentage errors mainly below 2%, with a mean absolute error equal to 1.35%. Moreover, the complete model can be executed

312 times faster than the real time, on a standard laptop, confirming it is particularly suitable for RT application.

Considering a possible implementation of the analytical model within a RT control strategy, the aim is to prevent turbine failure and the goal is that to have a high accuracy on the gas temperature estimation. In this context, the TC dynamics model is not necessary, and the output signal calculated by the analytical model is even more useful than a direct measurement since it avoids the risk of underestimating turbine inlet gas temperature. Future works the authors with this model will focus on the extension of the scaling factors to account for the effects of other control parameters that could vary during engine operation w.r.t. to nominal calibrated values, such as the Variable-Valve-Timing or Variable-Length intake runners. This approach will also be applied to a different type of engine, in order to verify its robustness and general validity.

References

1. Fu, H., Chen, X., Shilling, I., and Richardson, S., "A One-Dimensional Model for Heat Transfer in Engine Exhaust Systems," SAE Technical Paper 2005-01-0696, 2005, https://doi.org/10.4271/2005-01-0696.
2. Regulation (EU) 2019/631, European Commission, https://ec.europa.eu/clima/policies/transport/vehicles/regulation_en.
3. Zhao, F., “Technologies for Near-Zero-Emission Gasoline-Powered Vehicles”, Warrendale, Society of Automotive Engineers, Inc., 2006), 10.4271/R-359, ISBN 978-0-7680-4301-3.
4. Eriksson, L., "Mean Value Models for Exhaust System Temperatures," SAE Technical Paper 2002-01-0374, 2002, https://doi.org/10.4271/2002-01-0374.
5. Nasser, S. and Playfoot, B., "A Turbocharger Selection Computer Model," SAE Technical Paper 1999-01-0559, 1999, https://doi.org/10.4271/1999-01-0559.
6. Fulton, B., Van Nieuwstadt, M., Petrovic, S., and Roettger, D., "Exhaust Manifold Temperature Observer Model," SAE Technical Paper 2014-01-1155, 2014, doi:10.4271/2014-01-1155.
7. Dahlstrom, J., Andersson, O., Tuner, M., and Persson, H., “Experimental Comparison of Heat Losses in Stepped-Bowl and Re-Entrant Combustion Chambers in a Light Duty Diesel Engine,” SAE Technical Paper 2016-01-0732, 2016, doi:10.4271/2016-01-0732.
8. Olmeda, P., Martin, J., Garcia, A., Blanco, D. et al., “Evaluation of EGR Effect on the Global Energy Balance of a High Speed DI Diesel Engine,” SAE Technical Paper 2016- 01-0646, 2016, doi:10.4271/2016-01-0646.
9. Smith, L., Preston, W., Dowd, G., Taylor, O. et al., “Application of a First Law Heat Balance Method to a Turbocharged Automotive Diesel Engine,” SAE Technical Paper 2009-01-2744, 2009, doi:10.4271/2009-01-2744.
10. Brusa, A., Cavina, N., Rojo, N., Cucchi, M. et al., “Development and Validation of a Control-Oriented Analytic Engine Simulator,” SAE Technical Paper 2019-24-0002, 2019, doi:10.4271/2019-24-0002.
11. Malbec, L., Le Berr, F., Richard, S., Font, G. et al., "Modelling Turbocharged Spark-Ignition Engines: Towards Predictive Real Time Simulators," SAE Technical Paper 2009-01-0675, 2009, doi:10.4271/2009-01-0675.
12. Martin, D. and Rocci, B., "Virtual Exhaust Gas Temperature Measurement," SAE Technical Paper 2017-01-1065, 2017, doi:10.4271/2017-01-1065.
13. Son, S. and Kolasa, A., "Estimating Actual Exhaust Gas Temperature from Raw Thermocouple Measurements Acquired During Transient and Steady State Engine Dynamometer Tests," SAE Technical Paper 2007-01-0335, 2007, https://doi.org/10.4271/2007-01-0335.
14. S. V. Patankar, “Numerical Heat Transfer and Fluid Flow”, 1980, ISBN: 978-0070487406.
15. Cavina, N., "Measurement of Exhaust Gas Temperatures: Theoretical and Experimental Analysis", Proceedings of the ASME 2002 Internal Combustion Engine Division Fall Technical Conference, New Orleans, Louisiana, USA, September 8–11, 2002, pp. 557-565, ASME, https://doi.org/10.1115/ICEF2002-539.
16. Papaioannou, N., Leach, F., and Davy, M., “Effect of Thermocouple Size on the Measurement of Exhaust Gas Temperature in Internal Combustion Engines,” SAE Technical Paper 2018-01-1765, 2018, doi:10.4271/2018-01-1765.
17. C. D. Henning and R. Parker, “Transient response of an intrinsic thermocouple”, J. Heat Transfer. May 1967, 89(2): 146-152, https://doi.org/10.1115/1.3614337.
18. Gat, U., Kammer, D., Hahn, O. J., “The effect of temperature dependent properties on transient measurement with intrinsic thermocouple”, International Journal of Heat and Mass Transfer, Volume 18, Issue 12, December 1975, Pages 1337-1342, https://doi.org/10.1016/0017-9310(75)90246-X.
19. Matlab Documentation, The Mathworks.
20. Ravaglioli, V., Moro, D., Serra, G., and Ponti, F., "MFB50 On-Board Evaluation Based on a Zero-Dimensional ROHR Model," SAE Technical Paper 2011-01-1420, 2011, https://doi.org/10.4271/2011-01-1420.
21. Cavina, N., Migliore, F., Carmignani, L., and Di Palma, S., "Development of a Control-Oriented Engine Model Including Wave Action Effects," SAE Technical Paper 2009-24-0107, 2009, https://doi.org/10.4271/2009-24-0107.
22. Boiarciuc, A. and Floch, A., "Evaluation of a 0D Phenomenological SI Combustion Model," SAE Technical Paper 2011-01-1894, 2011, https://doi.org/10.4271/2011-01-1894.
23. Dekraker, P., Barba, D., Moskalik, A., and Butters, K., “Constructing Engine Maps for Full Vehicle Simulation Modeling”, SAE Technical Paper 2018-01-1412, 2018, doi:10.4271/2018-01-1412.
24. Finesso, R., Spessa, E., Yang, Y., Conte, G. et al., "Neural-Network Based Approach for Real-Time Control of BMEP and MFB50 in a Euro 6 Diesel Engine," SAE Technical Paper 2017-24-0068, 2017, doi:10.4271/2017-24-0068.
25. Brusca, S., Lanzafame, R., and Messina, M., "A Combustion Model for ICE by Means of Neural Network," SAE Technical Paper 2005-01-2110, 2005, https://doi.org/10.4271/2005-01-2110.
26. Trindade, W. and Santos, R., "Combustion Modeling Applied to Engines Using a 1D Simulation Code," SAE Technical Paper 2016-36-0347, 2016, https://doi.org/10.4271/2016-36-0347.
27. Bozza, F., Fontana, G., Galloni, E., and Torella, E., "3D-1D Analyses of the Turbulent Flow Field, Burning Speed and Knock Occurrence in a Turbocharged SI Engine," SAE Technical Paper 2007-24-0029, 2007, https://doi.org/10.4271/2007-24-0029.
28. Cavina, N., Rojo, N., Businaro, A., Brusa, A. et al., "Investigation of Water Injection Effects on Combustion Characteristics of a GDI TC Engine", *SAE Int. J. Engines* 10(4):2017, doi:10.4271/2017-24-0052.

29. Lee, S.-Y., Andert, J., Pischinger, S., Ehrly, M. et al., “Scalable Mean Value Modeling for Real-Time Engine Simulations with Improved Consistency and Adaptability,” SAE Technical Paper 2019-01-0195, 2019, doi:10.4271/2019-01-0195.
30. Pasternak, M., Mauss, F., Xavier, F., Rieß, M. et al., "0D/3D Simulations of Combustion in Gasoline Engines Operated with Multiple Spark Plug Technology", SAE Technical Paper 2015-01-1243, 2015, doi:10.4271/2015-01-1243.

Definitions/Abbreviations

AFR	Air-to-Fuel Ratio
ANN	Artificial Neural Network
CA	Crank Angle
CHR	Cumulative Heat Release
ECU	Engine Control Unit
EL	Engine Load
ES	Engine Speed
GDI	Gasoline Direct Injection
IMEP	Indicating Mean Effective Pressure
MA	Moving Average
MFB50	50% of Mass Fraction Burned
MIMS	Mineral-Insulated-Metal-Sheathed
PMAX	Maximum In-Cylinder Pressure
RAM	Random Access Memory
RCP	Rapid Control Prototyping
RMSE	Root Mean Squared Error
RT	Real Time
SA	Spark Advance
SI	Spark Ignition
TC	Thermocouple